

Comprehensive phenotyping combined with multi-omics of *Salmonella* Infantis and its H₂S negative variant - Resolving adaption mechanisms to environmental changes

Victoria Drauch^{a,*} , Nicola Palmieri^a, Joachim Spersger^b, Karin Hummel^c, Marlene Brandstetter^d, Christian Kornschöber^e, Michael Hess^a, Claudia Hess^{a,1}

^a Clinic for Poultry and Fish Medicine, Department for Farm Animals and Veterinary Public Health, University of Veterinary Medicine Vienna, Veterinärplatz 1, 1210, Vienna, Austria

^b Institute of Microbiology, Department of Biological Sciences and Pathobiology, University of Veterinary Medicine Vienna, Veterinärplatz 1, 1210, Vienna, Austria

^c VetCore Facility, Mass Spectrometry, University of Veterinary Medicine Vienna, Veterinärplatz 1, 1210, Vienna, Austria

^d Vienna Biocenter Core Facilities GmbH, EM Facility, 1030, Vienna, Austria

^e National Reference Centre for Salmonella, AGES, Beethovenstrasse 6, 8010, Graz, Austria

ARTICLE INFO

Keywords:

Salmonella
Salmonella Infantis
Atypical colony variant
Multi-omics
Adaption
Environmental changes

ABSTRACT

The zoonotic pathogen *S. Infantis* is of emerging importance, making detection in poultry critical. Phenotypic changes, which are significant for standardized control programs via EN/ISO 6579–1:2017, could lead to pathogens remaining undetected, increasing the risk of food-borne outbreaks. This study investigates an *S. Infantis* strain with both normal growth (NCP) and atypical H₂S-negative colony variant (ACV) from an Austrian broiler farm. NCP and ACV underwent comprehensive analyses, including stability tests, electron microscopy, whole-genome sequencing, transcriptomics, and proteomics. Our findings demonstrate a stable atypical colony variant exhibiting acquired resistance against cefoxitin in ACV. Genomic analysis identified 9 single nucleotide polymorphisms (SNPs) and two deletions, affecting genes involved in porphyrin and sulfur metabolism. Key factors were a mutation disrupting *cysG*, which is essential for siroheme biosynthesis and a vital cofactor in sulfur metabolism, and a stop codon in *menD* (2-oxoglutarate decarboxylase), crucial for small colony variant appearance. Consequently, we hypothesize that these mutations lead to a deficiency in siroheme, as well as anaerobic sulfur respiration altogether resulting in the H₂S-negative phenotype. Functional network analysis highlighted compensatory upregulation of alternative metabolic pathways, including nitrate metabolism, propanoate metabolism and mixed-acid fermentation, which may aid ACV's persistence and adaptation under anaerobic conditions. Reduced flagellin expression suggests a mechanism for immune evasion. These genetic and metabolic adaptations likely respond to environmental stressors, such as oxidative stress from disinfectants or antimicrobial pressure, leading to the emergence of the H₂S-negative phenotype. Consequently, this study provides insights into the genetic and biochemical adaptations of an atypical *S. Infantis* variant.

1. Introduction

Salmonella (*S.*) *enterica* subsp. *enterica* is the causative agent of salmonellosis, the second most reported foodborne gastrointestinal infection in the European Union (EU) (EFSA and ECDC, 2024). To combat salmonellosis, the EU implemented enhanced food safety regulations and control programs, resulting in a stabilization of infection rates over recent years (EFSA and ECDC, 2024). However, the

distribution of serovars in humans and poultry has shifted over the last few years. The prevalence of the two main target serovars, *S. Enteritidis* and *S. Typhimurium*, has decreased in humans and in poultry due to implementation of strict control programs, e.g. mandatory vaccinations of breeders and layers against *S. Enteritidis*, while other serovars became more prevalent. Since 2014, there has been an increase in *S. Infantis*, now the most isolated *Salmonella* serovar in broiler production systems (EFSA and ECDC, 2024). In parallel, a global increased

* Corresponding author.

E-mail address: Victoria.drauch@vetmeduni.ac.at (V. Drauch).

¹ Present Address: LVA, Magdeburggasse 10, 3400 Klosterneuburg, Austria.

incidence of this serovar has been reported associated with the emergence of multidrug-resistant (MDR) strains, which possess a mega-plasmid containing antimicrobial resistance genes and enhancing adherence and fitness, the so-called pESI plasmid (Alvarez et al., 2023).

Phenotypic heterogeneity in *Salmonella*, often due to genetic changes like SNPs, has been well-documented and can occur even in genetically identical cells (Ackermann, 2015). Such changes are adaptation mechanisms in response to environmental factors, acidic conditions or antimicrobial exposure (Ghoshal et al., 2023; Zhou et al., 2023a,b). Additionally, phenotypic changes can result from a shift in lifestyle from extracellular to intracellular (Liu et al., 2024; Powers et al., 2021; Wang et al., 2022). Screening of Austrian *S. Infantis* isolates showed substantial phenotypic variations (Hess et al., 2023). For the first time we present the identification of a *S. Infantis* that exhibited both a normal colony phenotype (NCP) and an atypical colony appearance lacking H₂S production (atypical colony variant, ACV).

Such atypical variants are of public health concern as they might evade detection employing standardized monitoring programs. In 2019, an outbreak of salmonellosis was reported in Sweden caused by an H₂S-negative *S. Typhimurium* (Colombe et al., 2019), which led to 82 nationwide cases within two months. The phenotypic variation was suspected as a possible cause for the outbreak, as H₂S production is a key feature in *Salmonella* detection using EN/ISO 6579-1:2017 standards.

The lack of H₂S production has been observed in various *Salmonella* serovars and the cause for the variation is attributed in the majority of cases to missense mutations in genes of the *phs* (production of hydrogen sulfide) operon or even absence of one of these genes (Kovac et al., 2017; Mourão et al., 2020; Müştak et al., 2020; Sakano et al., 2013; Wu et al., 2016; Xie et al., 2018; Yi et al., 2014). The *phs* operon is crucial for the reduction of thiosulfate to hydrogen sulfide, comprising three genes (*phsA*, *phsB*, and *phsC*) that encode thiosulfate reductases. However, in a study that analysed 46 H₂S-negative isolates from China, it was found that only 24 of the 46 isolates had mutations in the *phs* operon indicating that other genetic mechanisms must also contribute to this phenotype (Xie et al., 2018). Other genetic alterations responsible for the H₂S-negative phenotype have also been identified. For example, a missense mutation in *cysJ* (sulfite reductase, beta subunit) was reported in *S. Infantis* (Lee et al., 2020), while mutations in *tetR* (putative transcriptional regulator, TetR family), *moaC* (molybdenum cofactor biosynthesis protein C) and *sph* (streptomycin phosphotransferase) have been associated with H₂S-negative isolates of *S. Kentucky* (Albert et al., 2014). Interestingly, H₂S-negative *Salmonella* isolates have been primarily reported from 2013 onwards, with most H₂S-negative *S. Infantis* isolates originating from Asia (Sakano et al., 2013; Xie et al., 2018; Yi et al., 2014). Recently, reports of H₂S-negative *Salmonella* have also emerged in Europe (Colombe et al., 2019; Mourão et al., 2020; Müştak et al., 2020).

However, these investigations have primarily focused on single genes or specific pathways. Here, for the first time, we applied a multi-omics approach—combining whole-genome sequencing, transcriptomics, and proteomics—to comprehensively elucidate the genetic and biochemical underpinnings of the H₂S-negative phenotype in *S. Infantis*.

2. Material and methods

2.1. Bacterial strains, growth behaviour, stability and antimicrobial resistance pattern

During the mandatory routine testing using the standardized test method ISO 6579-1:2017 (EN ISO 6579-1, 2017) the *Salmonella* strain “PA-19/26029” was isolated in 2019 from a boot swab derived from a broiler farm located in Austria. Culturing this strain on XLD revealed, besides the typical black colonies which are considered as the normal colony phenotype (NCP) of PA-19/26029, also colonies lacking H₂S production and thus presenting themselves as transparent colonies

designated from now on as atypical colony variant (ACV) of PA-19/26029. The Kauffmann-White-Le Minor scheme was applied for serotyping and revealed the presence of *S. Infantis*. Both phenotypes (NCP and ACV) were tested for their growth characteristics and colony morphology on four additional agar plates: Columbia Agar with 5% sheep blood (COS, BioMerieux, Vienna, Austria) and MacConkey Agar (MCK, NEOGEN, Lansing, MI, USA), both commonly used in routine diagnostics, and Brilliant-green Phenol-red Lactose Sucrose Agar (BPLS, Bertoni, Vienna, Austria) and Modified Semisolid Rappaport Vassiliadis Agar (MSRV, Merck, Darmstadt, Germany) which are used, besides XLD, for the detection of *Salmonella* according to the ISO 6579-1:2017 (EN ISO 6579-1, 2017). One colony of each H₂S phenotype was transferred into 10 ml of Luria-Bertani (LB) broth (Thermo Fischer Scientific, Carlsbad, CA, USA), incubated at 37 °C under aerobic conditions in a shaking incubator (120 rpm) for 24 h. Cultures were then plated onto three different solid agars (COS, MCK and BPLS) using the three-phase streaking method. Plates were incubated at 37 °C under aerobic conditions for 24 h and colonies were evaluated for their shape, colour and size. For the semisolid MSRV agar one drop of the bacterial suspension was inoculated in the centre of the plate, incubated at 42 °C under aerobic conditions and the presence of swarming behaviour was evaluated after 24 h and 48 h.

Additionally, stability and purity of both phenotypes (NCP and ACV) were evaluated by culturing them on XLD followed by transfer of a single colony into 10 ml LB broth, incubated at 37 °C under aerobic conditions with an agitation of 120 rpm for 24 h. Serial dilutions were then plated onto XLD to evaluate the phenotype of produced colonies and approve allocated growth characteristics. Single colonies were picked, and the procedure repeated twice to confirm phenotypic stability of NCP and ACV.

The broth microdilution method was performed to assess the antimicrobial susceptibility patterns of both phenotypes (NCP und ACV) according to Clinical & Laboratory Standards Institute (CLSI) supplement VET01 (CLSI, 2015) using a MICRONAUT-S Austria Poultry plate (MERLIN Diagnostika GmbH, Bornheim-Hersel, Germany). Supplementary Table 1 shows the antimicrobials tested together with the corresponding concentrations and cut off values. The bacterial test suspensions were prepared according to the manufacturer’s instructions. Briefly, from a 5 ml bacterial suspension (McFarland standard 0.5) 50 µl were transferred into 11 ml of Müller-Hinton broth (Merck, Vienna, Austria) and mixed well. 100 µl of this mixture was put into each well of the microtiter plate and the plate was incubated aerobically at 37 °C. After 24 h the results were measured using the MCN6 Software version 6.00 release 72 (MERLIN Diagnostika GmbH, Bornheim-Hersel, Germany).

2.2. Electron microscopy

One colony from each phenotype (NCP and ACV) was picked from XLD agar and transferred in 10 ml LB broth and incubated at 37 °C under aerobic conditions with agitation (120 rpm) overnight. On the next day 50 µl of the bacterial suspension were transferred to 25 ml of LB broth and incubated again at 37 °C under aerobic conditions with agitation for exactly 4 h. For washing, bacterial suspensions were centrifuged at 5000 rpm for 10 min at 4 °C, supernatant was discharged, and the cell pellet was resuspended in phosphate-buffered saline (PBS, GIBCO, Paisley, UK). The washing was repeated, and the cell pellet was resuspended with a final volume of 50 ml PBS to achieve a concentration of 10⁶ CFU/ml and kept on ice till the negative staining procedure was performed. A 4 µl drop of sample was applied to the carbon side of carbon-coated hexagonal 400 mesh Cu/Pd grids (Agar Scientific, Rotham, UK). The carbon-film was self-made in an Edwards Auto 306 high vacuum evaporator (Edwards, Burgess Hill, UK) and the coated grids were glow-discharged for 1 min in a Bal-Tec SCD 005 sputter coater (Bal-Tec, Balzers, Liechtenstein) at 20 mA prior to staining to increase hydrophilicity. During the incubation time of 1 min, bacteria

attached to the carbon film. Afterwards, the excess sample was removed with a filter paper (Whatman No.1, Merck, Darmstadt, Germany), and immediately replaced by a 4 µl drop of stain. The drop was removed without incubation time. This step was performed as a washing step, to rinse off any unbound bacteria from the carbon film. Subsequently a fresh drop of stain was added. Again, the stain was removed without allowing the sample to incubate and the grid was left to dry for several minutes. The stain used in this experiment was 0.25% phosphotungstic acid (Merck, Darmstadt, Germany) in water with the pH adjusted to 7. The standard approach, incubating in stain for 1 min, was resulting in a very strong contrast, that made imaging of the flagella difficult. Reducing the incubation time to a minimum (approx. 15 s) helped. Both 2% aqueous uranyl acetate (Merck, Darmstadt, Germany) at pH4 and 2% phosphotungstic acid were tested previously and considered not suitable as the staining was likewise too strong, therefore it was chosen to dilute the stain. Grids were inspected in an FEI Morgagni 268D transmission electron microscope (previously FEI; now Thermo Fisher Scientific, Eindhoven, The Netherlands), operated at 80 kV. Examined regions on the grids were selected randomly. Digital images were acquired using a Mega View III CCD camera (Olympus-SIS, Münster, Germany).

2.3. DNA extraction

High molecular weight DNA was extracted with a protocol described by Sambrook and Russel (1982) and adapted from Josh Quick (2018). Briefly, overnight bacterial suspension was pelleted, resuspended and mixed with 10 ml of Tris-Lysis Buffer. After 1 h of incubation at 37 °C with end-to-end rotation, 100 µl of Proteinase K was added and mixed by inversion. This was followed by another incubation at 50 °C for 2 h, with inversion every 30 min. The viscous lysate was distributed into two falcon tubes with phase-lock gel and 5 ml of TE-saturated phenol per tube was added. Aqueous phase was obtained with the help of a Hula-Mixer and centrifugation and 4 ml of 5 M ammonium acetate as well as 30 ml of ice-cold ethanol (99%) were added. The DNA started precipitating and was stored at -20 °C. After five days samples were thawed and centrifuged at 10,000×g for 5 min. Supernatant was removed and 30 ml of ice-cold ethanol (70%) was added. Centrifugation and removal of supernatant was repeated two times adding 1 ml of ice-cold ethanol (70%). After the last removal of supernatant, the tube was kept open at room temperature for 15 min to enable evaporation of leftover ethanol. Then, 100 µl of elution buffer (10 mM Tris-Cl, pH 8.0) with 0.02% Triton X-100 was added and incubated without mixing at 4 °C for two days to allow the pellet to fully resuspend.

2.4. Illumina and Nanopore sequencing

For Nanopore MinION sequencing (Oxford Nanopore Technologies, Oxford, UK) the Ligation Sequencing Kit V14 was applied for library preparation and sequencing was performed for 48 h using a R10.4.1 flow cell. Real-time base calling was performed using MinKNOW operating software (version 24.02.6) with integrated Guppy data processing tool. Genomic DNA was additionally sequenced on an Illumina MiniSeq platform after library preparation using the Nextera™ DNA Flex Library Prep Kit. Genome assembly of Illumina short reads along with Nanopore long reads was performed in hybrid assembly mode of the Unicycler pipeline version 0.4.8 (<https://github.com/rrwick/Unicycler/>) with default settings (-min_fasta_length 100, -keep 1, -mode normal -linear_seqs 0) (Wick et al., 2017) resulting in a completed and circularized chromosome and a single plasmid for each of the sequenced phenotypes (NCP and ACV). The genomes of both isolates were submitted to NCBI under the accession numbers PRJNA1149069 for NCP and PRJNA1149073 for ACV.

2.5. Genome annotation

The genomes of the *Salmonella* Infantis phenotype NCP and ACV were annotated using PROKKA (Seeman, 2014) with the following parameters: -genus *Salmonella*, -species enterica, -strain NCP, -outdir NCP, -prefix NCP, -compliant, and -cpus 16. These settings ensured compliance with GenBank standards and detailed genus, species, and strain information. Additionally, the genomes were screened for the presence of the emerging megaplasmid pESI by aligning the sequence of the pESI plasmid from isolate 119944 (accession NZ_CP047882.1) to both NCP and ACV genomes using the Whole Genome Alignment tool from CLC Genomics Workbench v.25 (<https://digitalinsights.qiagen.com/>). Following annotation, we used OMA (Orthologous Matrix) (Altenhoff et al., 2019) with default parameters to convert the PROKKA gene IDs of NCP and ACV to the reference gene IDs of the *Salmonella* typhimurium LT2 strain. OMA takes the proteins of the three strains as input. This step is crucial as it allows us to leverage online databases such as KEGG and STRING, which contain gene IDs for the LT2 strain, to extract functional information for candidate genes linked to our atypical colony phenotype. Panaroo (Tonkin-Hill et al., 2020) was then utilized to generate a gene presence-absence matrix, incorporating the reference strain LT2 along with the annotated genomes of NCP and ACV. Panaroo was configured in strict mode (-mode strict) with consensus-based removal of dubious genes (-remove_by_consensus True) to enhance the accuracy of the gene matrix. The primary aim of using Panaroo was to identify putative gained or lost genes in the ACV. For the identification of single nucleotide polymorphisms (SNPs), we first identified closely related genomes to NCP using the Similar Genome Finder tool from the BV-BRC platform. This tool was run using the NCP genome as input, and the closest 50 genomes were retrieved. An initial phylogenetic tree was constructed, and six genomes clustering with NCP and ACV were retained for further analysis (Infantis_355021_595_811, 437982_59201_1362, Infantis_strain_SB017_595_401, 32020501-2019-00041_2819700_3, Infantis_strain_UZH_SAL-111-10_595_108 and Infantis_strain_MRS-17_00712_595_777). The genomes of NCP, ACV, LT2, and the six selected closely related genomes were aligned using Parsnp (Treangen et al., 2014) with the following parameters: c, -p 16, -d genomes, -g LT2, and -x. Following the alignment, harvesttools (Treangen et al., 2014) was used to generate a VCF file cataloguing the SNPs. Filtering was then applied to isolate SNPs unique to ACV, excluding those shared with ancestral genomes. To provide functional annotations for these SNPs, SnpEff (Cingolani et al., 2012) was used by first building a database for the reference strain (*build -genbank -v Salmonella_Typhimurium_LT2*) and then annotating the VCF file (*ann -v Salmonella_Typhimurium_LT2*). To further assess the potential impact of these mutations, SIFT (Sorting Intolerant From Tolerant) (Ng and Henikoff, 2003) analysis was performed to predict whether the amino acid substitutions affect protein function.

2.6. RNA extraction

RNA extraction was performed from bacterial suspension using RNeasy Mini Kit (Qiagen). Phenotypes were grown overnight in 25 ml LB Broth at 37 °C under aerobic conditions in a shaking incubator (150 rpm). On the next day 50 µl of the overnight culture were transferred to fresh 25 ml of LB Broth and incubated at 37 °C under aerobic conditions in a shaking incubator (150 rpm) for 3 h reaching a growth of 10⁸ CFU/ml which was confirmed via CFU count. 5 ml of fresh bacterial suspension were centrifuged for 6 min at 4000 rpm. The supernatant was discarded, and the pellet was washed in 700 µl PBS and snap frozen in liquid nitrogen. 200 µl TE-Buffer including 15 mg lysozym/ml was added to the pellet as well as 10 µl Proteinase K, vortexed for 10 s and incubated at room temperature (23–25 °C) on a shaking incubator (750 rpm) for 10 min. RLT Buffer was prepared containing 10 µl β-mercaptoethanol and RNA extraction was continued according to the protocol of the RNeasy Mini Kit. RNA concentration and quality was measured

via RNA ScreenTape Assay to ensure RIN >7 and DV200 > 70%.

2.7. Transcriptomic data analysis

Total RNA was extracted from the samples and subjected to sequencing on the Illumina platform (NextSeq550Medium), generating 150 bp paired end reads. The raw reads were processed using cutadapt to remove adapter sequences and low-quality bases, with the following parameters: adapters (AGATCGGAAGAGC), a minimum read length of 20 bp, and parallel processing with 16 threads. The trimmed reads were then loaded into CLC Genomics Workbench 23 for RNA-seq analysis (<https://digitalinsights.qiagen.com/>). The reference transcripts for phenotypes NCP and ACV were obtained from previously conducted PROKKA annotations. Using the RNA-Seq Analysis module in CLC, gene expression levels were quantified, and expression tables were generated for each sample. Each table included the following columns: PROKKA Gene_ID, TPM (Transcripts Per Million), Unique gene reads, and Total gene reads. To integrate the data, expression tables from all samples were exported and merged using R. The combination of expression data for NCP and ACV was facilitated by the previously generated table from the OMA tool, which provided the mapping between the LT2 strain gene IDs and the PROKKA gene IDs from NCP and ACV. The resulting merged table contained comprehensive expression data for both phenotypes. Differential expression analysis was conducted using the DESeq2 package (Love et al., 2014) in R to identify genes with significant expression differences between ACV and NCP. Raw read counts for each gene were extracted from the merged expression table and used as input for the R package DESeq2. The analysis involved constructing a count matrix, creating a sample information table indicating the conditions (NCP or ACV), and generating a DESeqDataSet object. The DESeq2 pipeline was executed to normalize the data and estimate dispersion. Genes with a log₂ fold change between ACV and NCP greater than or equal to 1.5 and an adjusted *p*-value less than 0.05 were considered as differentially expressed.

2.8. Protein extraction and LC-MS data acquisition

For each phenotype three biological replicates were produced by culturing onto a XLD plate incubated at 37 °C under aerobic conditions for 24 h. Bacterial colonies were transferred into a tube containing 500 µl Urea/Thiourea Lysis buffer and 25 µl 1 M dithiothreitol. Then 50 µl protease-inhibitor were added, vortexed and kept on ice. Samples were sonicated (power: 80%, 3 cycles à 10 s) and afterwards centrifuged with 10000 rcf at 4 °C for 7 min. Supernatant containing the extracted proteins was pipetted into a new tube. Protein concentration was measured with the use of 2-D Quant kit (Sigma-Aldrich Handels GmbH, Vienna, Austria) according to the manufacturer's instructions. Thirty microgram of protein lysate were transferred onto a 10 kD Pall Nanosep ultrafiltration unit (Pall Corporation, NY, USA) for tryptic digest applying a filter-aided sample preparation protocol according to Mayr et al. (2024). Cleanup of extracted peptides was performed using Pierce C18 spin columns as described by the manufacturer (Thermo Fisher Scientific, MA, USA).

Peptide analysis was accomplished on a nano-HPLC Ultimate 3000 RSLC system (Dionex) coupled to a high-resolution Q-Exactive HF Orbitrap mass spectrometer (Thermo Fisher Scientific) (Mayr et al., 2024). For quantitative analysis samples were injected in technical duplicates.

2.9. Qualitative and quantitative proteomic data analysis

For the identification of proteins, database searches of the acquired peptide spectra were performed using Proteome Discoverer Software 2.4.1.15 (Thermo Fisher Scientific). The protein databases used for the searches included the in-house annotated proteins from the two *Salmonella* Infantis isolates, as well as a common contaminant database

(www.thegpm.org/crap/) to be able to exclude contaminants from the final data analysis. The database searches were configured with the enzyme trypsin, allowing a maximum of two missed cleavage sites. Precursor mass tolerance was set at 10 ppm and fragment mass tolerance at 0.02 Da. The dynamic modifications included oxidation (+15.995 Da on methionine), deamidation (+0.984 Da on asparagine and glutamine), and several N-terminal modifications (acetylation, met-loss, and met-loss + acetyl). A static modification was set for carbamidomethyl (+57.021 Da on cysteine). Decoy database searches were conducted with a target false discovery rate (FDR) of 0.01 for strict criteria and 0.05 for relaxed criteria, at the peptide and protein level.

Intensity-based label-free quantification (LFQ) was performed based on protein abundance values (normalised to total area sums) generated with the Proteome Discoverer software. Before statistical analysis with R version 4.3.0 (R Core Team, 2023), normalised abundance values of the technical replicates were aggregated by the mean. To maintain high data quality, proteins with one or two missing abundance values within the three biological replicates were excluded from further data analysis. Abundance changes between the two groups were tested with a two-sample *t*-test. Proteins with significant changes in abundance level reported as up- or downregulated, are identified with more than two tryptic peptides and quantified with at least one unique peptide. Their fold change is higher/lower than ±1.5 log₂ fold with a *p*-value adjusted according to Benjamini-Hochberg for controlling the false discovery rate lower than 0.05.

2.10. Identification of candidate genes linked to a H₂S negative phenotype

To identify candidate genes associated with the atypical colony phenotype, we employed an integrative approach utilizing transcriptomics, proteomics, and genomic analyses. Initially, differentially expressed genes (DEGs) were identified from the RNA-seq data. Genes with a *p*-value <0.05 and an absolute log₂ fold change (log₂ FC) ≥ 1.5 were selected as significant DEGs. Similarly, differentially expressed proteins (DEPs) were identified from the proteomics data using the same threshold criteria (*p*-value <0.05 and absolute log₂FC ≥ 1.5). The union of DEGs from the transcriptomics data and DEPs from the proteomics data was used to construct the primary set of genes linked to the atypical phenotype.

Additionally, genes with SNPs or indels specific to ACV, including non-synonymous SNPs and premature stop codons, were incorporated into the final set of candidate genes. These mutations were selected based on their potential to significantly affect gene function. Functional annotations for the identified candidate genes were compiled using information from multiple databases and literature sources. These databases included KEGG, STRING, and UniProt, alongside relevant literature searches. Each gene was assigned a concise functional annotation string summarizing its biochemical pathway. To visualize the interactions and functional relationships of the candidate genes, the corresponding gene network was downloaded from the STRING database. This network, along with the functional annotation and log₂FC information from both transcriptomics and proteomics, was imported into Cytoscape (Shannon et al., 2003). Cytoscape was then used to generate annotated gene networks, providing a comprehensive overview of the candidate genes and their potential roles in the atypical colony phenotype.

3. Results

3.1. Growth behaviour on agar plates, phenotypic stability, antimicrobial susceptibility pattern and cell morphology

Picking single colonies of NCP and ACV and transferring onto XLD showed pure subcultures of a typical black phenotype and a transparent phenotype (Fig. 1). Determining the growth characteristics of both phenotypes (NCP and ACV) on four other agar plates (COS, MCK, BPLS

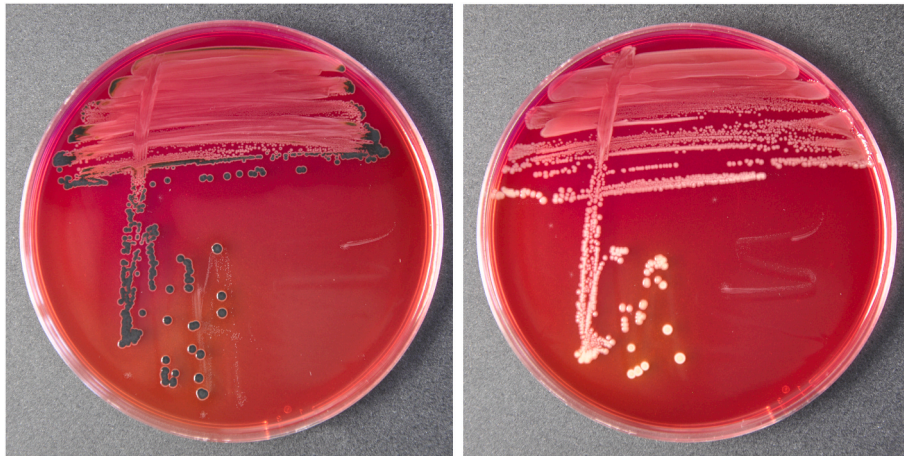


Fig. 1. Phenotype on XLD Agar of *Salmonella* Infantis NCP on the left compared to the ACV on the right missing the typical black coloration due to the lack of H₂S production.

and MSR/V) showed neither differences in colony morphology nor in motility.

Subculturing, dilution and single colony evaluation was performed and the above described typical and atypical phenotypes were shown to be stable. The antimicrobial susceptibility pattern evaluated via broth microdilution assay revealed the difference in one antimicrobial, namely ceftioxin, where the NCP showed a sensitive phenotype, and the ACV was resistant (Supplementary Table 2). Negative staining of the phenotypes did not show any significant difference in morphology regarding presence or length of flagella by electron microscopy (Fig. 2).

3.2. Genomics analysis

The genomes of *Salmonella* Infantis NCP and ACV were sequenced and assembled resulting in a completed circular chromosome (4.6 Mb; GenBank accession NCP: CP167167, ACV: CP167169) and a small plasmid (33 kb; GenBank accession NCP: CP167168, ACV: CP167170) for each of the phenotypes. To further characterize the plasmid, we performed a BLAST search against the pESI megaplasmid reference (SIN119944; Aviv et al., 2014) and found no significant hits, indicating the absence of pESI in both NCP and ACV. Table 1a provides an overview of the chromosome characteristics for both phenotypes, indicating minor differences in size and gene content between NCP and ACV. To establish the relationship between NCP and ACV, we constructed a phylogenetic tree using NCP, ACV, and six closely related genomes. The analysis showed that NCP and ACV cluster closely together, with ACV having a longer branch, indicating that ACV is derived from NCP (Supplementary Fig. 6).

To investigate the genetic basis of the phenotypic differences between NCP and ACV, we aligned the genomes of NCP, ACV, six closely

Table 1a

Chromosome characteristics of *Salmonella* Infantis NCP and ACV.

| Genome metric | NCP | ACV |
|---------------|---------|---------|
| Contigs | 1 | 1 |
| Size (bp) | 4617305 | 4617521 |
| CDS (total) | 4370 | 4371 |
| Gene (total) | 4491 | 4493 |
| rRNA | 22 | 22 |
| tRNA | 83 | 84 |
| ncRNA | 16 | 16 |

related strains, and the reference strain *Salmonella typhimurium* LT2. The alignment focused on the core genome, which constitutes 88% of the total genome, to identify mutations specific to ACV. We identified 15 SNPs unique to ACV, including 13 located within genes and 2 in intergenic regions. Among the gene-associated SNPs, 4 were synonymous, 7 were non-synonymous (missense variants), and 2 were stop-gained mutations. Additionally, we detected 2 single-base pair deletions in ACV that caused frameshifts, leading to premature stop codons. To focus on mutations with potential functional impact, we considered only the 7 missense variants, 2 stop-gained mutations, and 2 deletions, totaling 11 mutations affecting 11 distinct genes (Table 1b). SIFT analysis further indicated that 5 of the 7 missense variants are likely to impact protein function. The two single-base pair deletions were initially flagged as copy number variations (CNVs) by Panaroo due to gene splitting during annotation. However, a closer examination revealed that these were actually single-base pair deletions occurring within repetitive regions of the genes, leading to frameshifts that truncated the proteins. This caused PROKKA to annotate the affected genes in two parts, but this was an

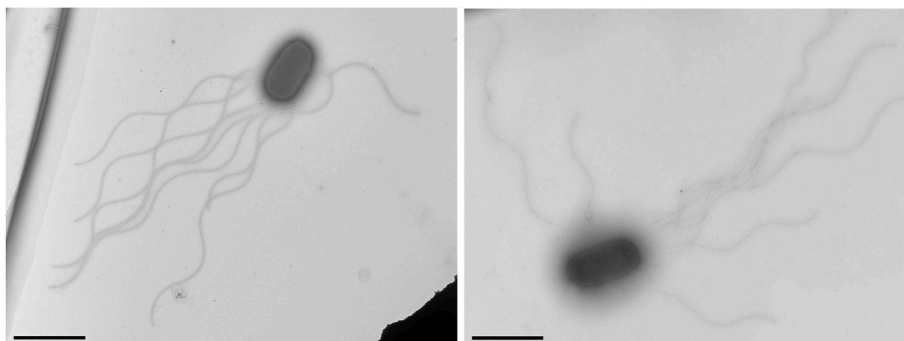


Fig. 2. Electron microscopy images of *Salmonella* Infantis NCP (left) and ACV (right). The scale bar represents a length of 2 μ m.

Table 1b

Identified genetic variations in *Salmonella* Infantis ACV compared to NCP with annotations relative to the reference strain LT2. It includes the gene IDs, gene function, type of mutation, genomic position, variant effect on the gene, and SIFT score.

| Gene ID | LT2 Gene ID | Gene description | Mutation type | Position | SNP annotation | Mutation | SIFT score |
|---------|-------------|---|-----------------|----------------|------------------|-------------|-------------------|
| ompF | STM0999 | outer membrane protein 1a | SNP | 1090506 | Missense variant | 124 Asp→Asn | 0.00 |
| dcm | STM1992 | similar to <i>E. coli</i> DNA cytosine methylase (AAC75027.1) | SNP | 2075000 | Missense variant | 253 Gly→Arg | 0.00 |
| menD | STM2309 | 2-oxoglutarate decarboxylase | SNP | 2416645 | Stop gained | – | – |
| yfeA | STM2410 | diguanylate cyclase/phosphodiesterase domain 2 | SNP | 2527302 | Missense variant | 482 Ser→Phe | 0.07 |
| ygbD | STM2841 | putative oxidoreductase | SNP | 2987412 | Missense variant | 301 Gly→Asp | 0.00 |
| cysG | STM3477 | siroheme synthase | SNP | 3628383 | Missense variant | 303 Asp→Ala | 0.00 |
| STM4440 | STM4440 | putative cytoplasmic protein | SNP | 4684022 | Missense variant | 22 Glu→Lys | – |
| rimI | STM4558 | modification of 30S ribosomal subunit protein S18 | SNP | 4813060 | Missense variant | 131 Pro→Leu | 0.00 ^a |
| sthE | STM4591 | putative major fimbrial subunit. | SNP | 4848744 | Stop gained | – | – |
| oadB | STM3351 | oxaloacetate decarboxylase beta chain | Deletion (1 bp) | – ^b | Stop gained | – | – |
| ccmF | STM2249 | similar to <i>E. coli</i> cytochrome c-type biogenesis protein (AAC75256.1) | Deletion (1 bp) | – ^b | Stop gained | – | – |

a Low confidence.

^b The deletions in *oadB* and *ccmF* have no position since they were detected through a custom alignment of the gene sequences using CLC.

artifact of the frameshift and did not represent true CNVs. As a result, the number of coding genes between NCP and ACV remains equivalent when considering only the functional portions of the genes.

3.3. Transcriptomics analysis

To understand the biochemical basis of the atypical colony phenotype observed in the ACV, we generated RNA-seq data for both the NCP and ACV, each with three biological replicates. The RNA-seq reads were mapped to the respective genomes, with the number of reads for each sample provided in [Supplementary Table 3](#). The number of reads per sample varied from 13 million to 22 million, reflecting high variability in coverage depth. Despite these differences, the percentage of expressed genes ranged from 87.7% to 89.6% and was very similar across all replicates ([Supplementary Table 3](#)), ensuring the reliability of the RNA-seq data for downstream analyses. The pairwise correlation plot of each replicate against each other showed a correlation range from 0.888 to 0.991 ([Supplementary Fig. 1](#)). The correlation within each phenotype was higher, ranging from 0.952 to 0.991, compared to the correlation between the phenotypes, which ranged from 0.888 to 0.943. The high within-phenotype correlation confirms the reproducibility and consistency of the RNA-seq data, suggesting that the observed differences in gene expression between NCP and ACV are likely due to genuine biological differences rather than technical variability. We performed differential expression analysis to identify genes with significant expression differences between NCP and ACV. Using a threshold of log₂ fold change ≥ 1.5 or ≤ -1.5 and an adjusted *p*-value < 0.05 , we identified 123 differentially expressed genes (DEGs), which accounts for 3.1% of the expressed genes ([Supplementary Fig. 2](#)).

3.4. Proteomics analysis

To understand the proteomic changes underlying the atypical colony phenotype in the ACV, we performed a proteomics analysis for both NCP and ACV, each with three biological replicates, obtaining data for 1901 proteins. The pairwise correlation plot among replicates ([Supplementary Fig. 3](#)) showed that the correlation within samples is higher, ranging from 0.986 to 0.997, while the correlation between samples is lower, ranging from 0.966 to 0.976. This indicates high consistency within replicates and genuine biological differences between NCP and ACV. Using a differential expression criterion of log₂ fold

change ≥ 1.5 or ≤ -1.5 and an adjusted *p*-value < 0.05 , we identified 79 differentially expressed proteins (DEPs), representing 4.1% of the total detected proteins ([Supplementary Fig. 4](#)).

3.5. Correlation of transcriptomics and proteomics data

To correlate transcriptomics and proteomics data, we first summarized the replicate data from each omics since there was no direct one-to-one match between transcriptomics and proteomics replicates. We computed the median log₂-transformed raw expression values from the triplicates to obtain a single value for each gene per phenotype (NCP and ACV). This method leveraged the high correlation within replicates to ensure reliable summary statistics. The resulting correlation coefficients were 0.38 for NCP and 0.36 for ACV ([Supplementary Fig. 5](#)), demonstrating a moderate correlation between RNA and protein expression levels for the phenotypes.

3.6. Identification of candidate genes linked to the atypical colony variant phenotype

To identify candidate genes associated with the atypical colony phenotype, we combined transcriptomics, proteomics, and genomic analyses and identified 204 candidate genes ([Supplementary Table 4](#)). Using the STRING database, we found that 172 of these genes are connected within a gene network, while 3 remain isolated. Of the 172 connected genes, 151 of them belong to a main large network, while 21 are distributed into five small networks, each with less than 10 genes ([Fig. 3](#)). Network topology analysis identified three highly connected nodes (hubs) within the main large network: *cysG* (siroheme synthase) with 21 connections, *adhE* (acetaldehyde dehydrogenase) with 15 connections and *putA* (plasma membrane proline dehydrogenase) with 10 connections. Hubs were defined as genes with at least 10 connections to genes not in the same functional cluster. The main hub is the downregulated *cysG* gene, which contains a missense variant and is crucial for siroheme biosynthesis and sulfur reduction. It connects to different clusters: at the top, it is linked to the upregulation of *ccm* genes (heme metabolism) and *nap*, *nar*, *nir* genes (nitrogen metabolism); to its left, it is associated with the upregulation of the *hyc* cluster (mixed-acid fermentation); and to the right, it connects to the upregulated *cbi* genes (porphyrin metabolism), the upregulated *pdu*, *yqhD* genes (propanediol metabolism), and the downregulated *eut* genes (ethanolamine

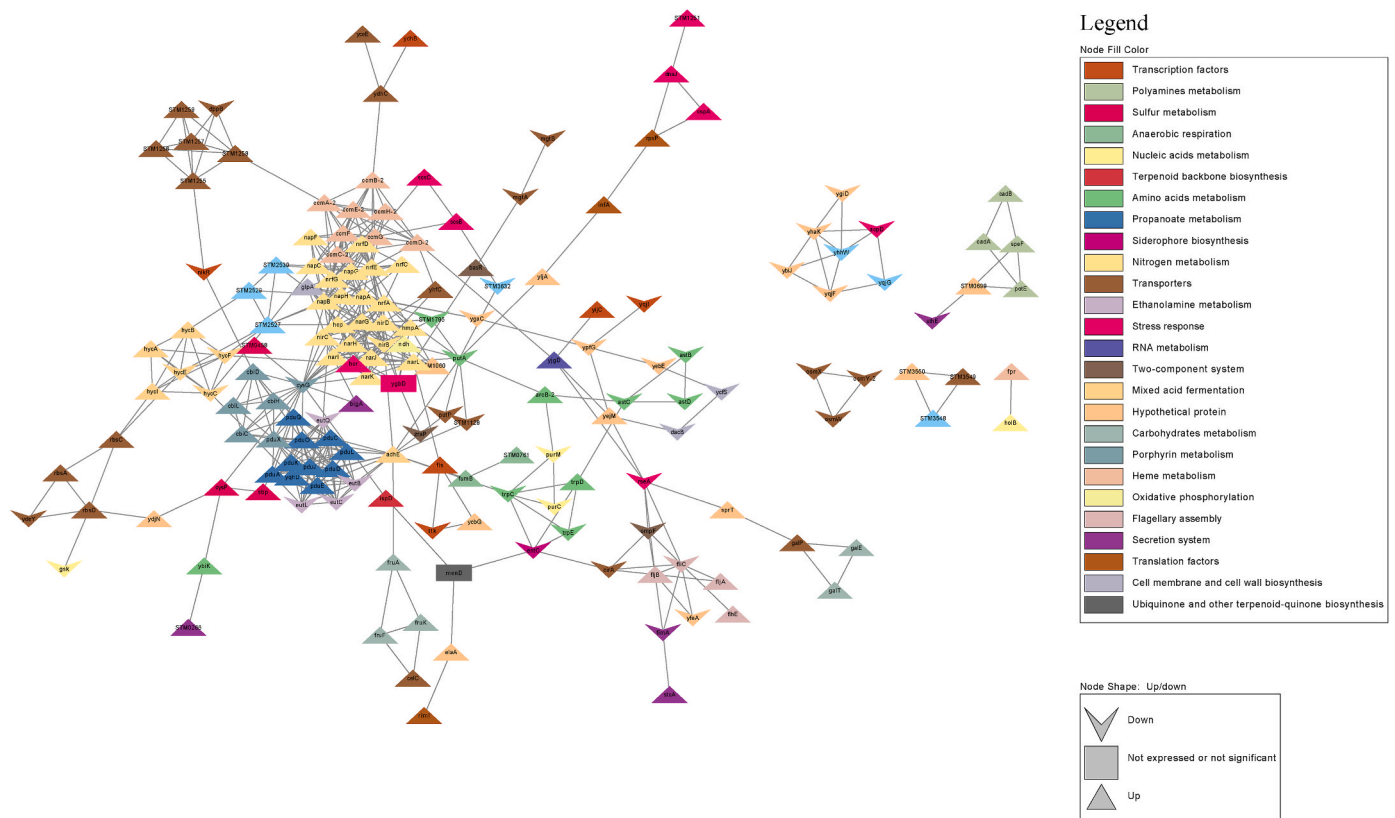


Fig. 3. Annotated gene network of 172 connected genes linked to the atypical colony phenotype.

The network was constructed using STRING database information and visualized in Cytoscape. Nodes represent genes, colored according to their associated metabolic pathways. Edges represent interactions between genes. Upregulated genes are marked with an upward triangle, while downregulated genes are marked with a downward V-shaped polygon. Classification of up/downregulation was based on \log_2FC values as follows: If both $\text{transcript}_{\log_2FC}$ and $\text{protein}_{\log_2FC}$ are available, genes are upregulated if both values are positive, and downregulated if both values are negative. If only $\text{protein}_{\log_2FC}$ is available, genes are upregulated if $\text{protein}_{\log_2FC} > 1.5$, and downregulated if $\text{protein}_{\log_2FC} < -1.5$. If only $\text{transcript}_{\log_2FC}$ is available, genes are upregulated if $\text{transcript}_{\log_2FC} > 1.5$, and downregulated if $\text{transcript}_{\log_2FC} < -1.5$.

metabolism). The second hub is the upregulated *adhE* gene, which encodes alcohol dehydrogenase essential for mixed-acid fermentation. It connects to the bottom with the upregulated *pdu*, *yqhD* genes (propanoate metabolism) and downregulated *eut* genes (ethanolamine metabolism), on top with the downregulated *putA* and *putP*, and to the right with the upregulated *fumB* (anaerobic respiration), *fru* genes (carbohydrate metabolism), and *celC* (transporter). The third hub is the *putA* gene, a trifunctional gene that is connected to the *pdu* and *yqhD* genes involved in propanoate metabolism. Additionally, it links to three uncharacterized genes: STM1128, STM3632, and *yljA*, as well as the transporter gene *putP*. Furthermore, *putA* is connected to the second hub, *adhE*, indicating a potential interaction or regulatory relationship between these hubs.

Fig. 4 shows transcript and protein \log_2FC in a heatmap. The heatmap highlights five genes whose proteomic data suggest they are proteins specific to the ACV phenotype, shown in dark red (ornithine carbamoyltransferase *arcB-2*, vitamin B12 adenosyl cobalamide precursor *cbiD*, 4-phosphocytidyl-2C-methyl-D-erythritol synthase *ispD*, TetR/AcrR family transcriptional repressor *yijC*, and site-specific DNA inversion stimulation factor *fis*), and one protein specific to the NCP phenotype, shown in dark blue (tartronic semialdehyde reductase *glxR*). The most abundant categories of genes, excluding hypothetical proteins, include transporters (24 genes), nitrogen metabolism (22 genes), amino acid metabolism (11 genes), and propanoate metabolism (10 genes).

4. Discussion

S. Infantis is an emerging zoonotic pathogen that has a strong affinity

to fast-growing broilers (EFSA and ECDC, 2024; Drauch et al., 2022). The increasing number of multidrug resistant isolates, as well as reports from the field indicating difficulties in eradication of *S. Infantis*, can be attributed to the presence of a megaplasmid designated pESI (Alba et al., 2020; Bezek et al., 2023; Drauch et al., 2020; McMillan et al., 2022). Besides this, *Salmonella* is also known to activate different adaptation mechanisms which can result in phenotypic heterogeneity (Grimbergen et al., 2015; Morawska et al., 2022). The present study focused on a *S. Infantis* isolate derived from an environmental sample of an Austrian broiler flock presenting a normal (H_2S -positive) colony phenotype (NCP) and an atypical (H_2S -negative) colony variant (ACV). Multi-omics analysis was used to explore genomic loci underlying the observed phenotypic variation.

In previous studies, the occurrence of H_2S -negative *Salmonella* isolates was mostly associated with mutations in the *phs* (production of hydrogen sulfide) operon (Mourão et al., 2020), but also other possible underlying mechanisms were suggested (Abd El Ghany et al., 2016; Albert et al., 2014). This is the fourth report of the occurrence of H_2S -negative *Salmonella* isolates in Europe, and to our knowledge the first H_2S -negative *Salmonella* isolate belonging to the serovar *Infantis* isolated in Europe (Colombe et al., 2019; Mourão et al., 2020; Müştak et al., 2020).

The coexistence of H_2S -negative and H_2S -positive *Salmonella* colonies from the same environment, as observed in our *S. Infantis* isolate from broilers, has also been reported in human-derived *Salmonella* isolates. Studies by Yi et al. (2014) and Albert et al. (2014) suggest that phenotypic variation can occur within a single bacterial isolate, which might explain the presence of both phenotypes in the strains we studied.

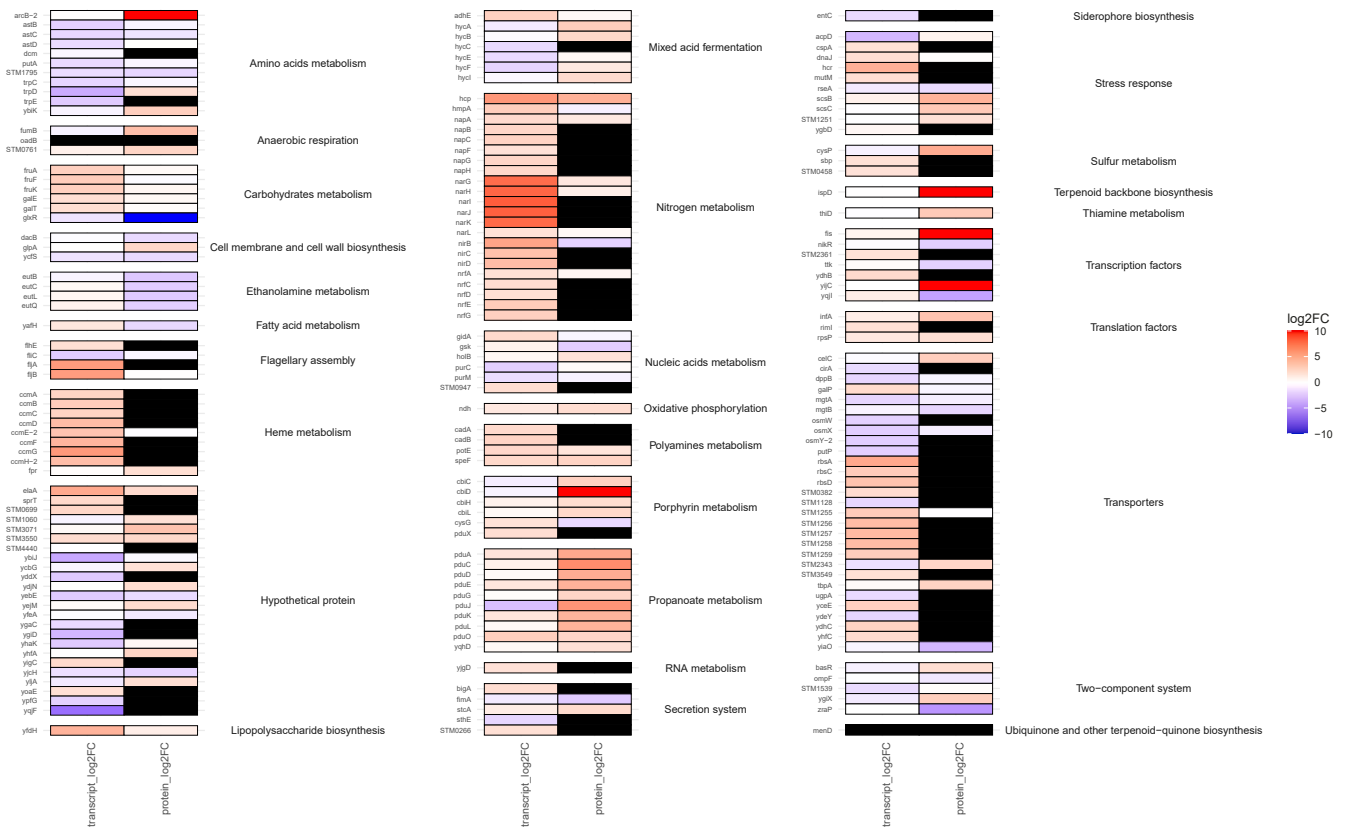


Fig. 4. Heatmap of transcript and protein log₂ fold changes (log₂FC) for 204 candidate genes linked to the atypical colony variant. Each cell represents the log₂FC for a specific gene, categorized by functional annotation. The blue-to-red color gradient indicates the magnitude of the log₂FC, with blue representing downregulation, red representing upregulation, and black indicating missing data. The gradient covers log₂FC values from -10 to +10, with values below -10 shown in dark blue and values above +10 shown in dark red. This choice was made to avoid central values of the distribution being indistinguishable from white, thus providing a clearer visual distinction between upregulated and downregulated genes.

Here, we confirmed that the colony characteristics of both the normal colony phenotype (NCP) and the atypical colony variant (ACV) phenotype are stably expressed over generations. Electron microscopy revealed no differences in the cell and flagella morphology between NCP and ACV. However, the antimicrobial resistance pattern showed a notable difference as the ACV proved resistance to the cephalosporin cefoxitin. Interestingly, Yi et al. (2014) also observed differences in antimicrobial resistance patterns, specifically within this group of antimicrobials, in their H₂S-negative ACV, whereas Albert et al. (2014) reported that the ACV had the same resistance profile as the corresponding NCP. These findings underscore the complexity of phenotypic variation and its implications for antimicrobial resistance and detection in clinical and environmental settings.

The megaplasmid pESI and its variations, known as pESI-like megaplasmids, have experienced a global spread within the last ten years in the *S. Infantis* population (Alvarez et al., 2023). However, neither NCP nor ACV contained a pESI or pESI-like megaplasmid. Despite this absence the results remain important, highlighting alternative mechanisms of adaptation, beyond megaplasmid-associated traits.

In total, 11 mutations in 11 genes were discovered by comparing the genomes of NCP and ACV, with cascading effects on several intertwined metabolic pathways. In the following paragraphs the role of these genes will be discussed and linked to possible underlying causes as well as functional impact as significant changes in bacterial metabolism which ultimately led to an H₂S-negative colony phenotype.

A SNP in the gene *menD* (2-oxoglutarate decarboxylase) resulted in a premature stop codon in ACV which may affect its function in the menaquinone biosynthesis. Menaquinones are involved in electron

transfer for anaerobic respiration in *Salmonella* and mutations in the *men* operon have been found to lead to a lack of H₂S production previously (Kwan and Barrett, 1983, 1984). In our proteomic data, a significant decrease was found in 1,4-dihydroxy-2-naphthoyl-CoA synthase, also known as *menB*, which could be a result of the stop codon identified in *menD*. This finding is supported by Clark and Barrett (1987), demonstrating that a *menB* mutant was only able to produce H₂S from sulfite but not from thiosulfate.

Connected to the *menD* mutation is a strong upregulation of *ispD*, which could have been triggered as a compensatory mechanism. The *ispD* gene encodes for 4-diphosphocytidyl-2C-methyl-D-erythritol synthase, an enzyme involved in the non-mevalonate pathway (MEP pathway) for isoprenoid biosynthesis. This pathway is crucial to produce isoprenoids, which are precursors for a variety of quinones, including ubiquinone (Meganathan and Kwon, 2009). Ubiquinone is essential for cellular energy production as it plays a key role in the electron transport chain. The upregulation of *ispD* could therefore be a cellular response to ensure adequate production of alternative quinones like ubiquinone, compensating for the disruption in menaquinone biosynthesis.

Furthermore, other atypical colony phenotypes such as small colony variants (SCVs) were shown to be caused by mutations in the *menD* gene leading to a deficiency in the electron transport (Proctor et al., 2006). A study on SCVs in *Enterobacteriaceae* revealed that each variant had at least one genomic change connected to oxidative respiration as well as iron acquisition and the cause of this phenotypic change is associated with the use of antimicrobials (Greninger et al., 2021).

Interestingly, a *menD* mutant was reported to be more persistent intracellularly in eukaryotic cells, indicating that the mutation leads to a

more persistent and chronic lifestyle (Bates et al., 2003; Cano et al., 2003). It has also been reported that some *Salmonella* SCVs show an increased ability for biofilm formation (Li et al., 2016) and that they can partially revert to normal growth (Drescher et al., 2019; Pr anting and Andersson, 2010). The exposure to antibiotics was shown to select for SCVs in different *Salmonella* serovars (Drescher et al., 2019) but in contrast to our findings SCVs were not stable. We conclude that the mutations in *menD* may not only lead to smaller colonies but can also influence H₂S production in *Salmonella* serovars due to its importance in the menaquinone biosynthesis and involvement in the electron transfer for anaerobic respiration.

Another SNP, resulting in a premature stop codon in ACV, was found in *sthE* encoding a putative major fimbrial subunit which was confirmed by transcriptomics showing a significant downregulation in the H₂S-negative phenotype. A knockout study of *sthE* in *S. Typhimurium* showed a significant decrease in biofilm forming capabilities (Eran et al., 2020). Weening et al. (2005) demonstrated that in mice a deletion in the *sth* operon of *S. Typhimurium* led to a decreased shedding behaviour, however host colonization was not affected. Downregulation of *sthE* is also connected with a uniform increase of transcriptomic and proteomic expression of genes involved in the polyamine metabolism (*potE*, *speF*, *cadBA*) which has recently been shown to play a role in stress response as well as in the survival of *S. Typhimurium* in macrophages (Nair et al., 2024). The *cadBA* operon is regulated by *cadC*, an acid-inducible transcription factor known to play an important role in bacterial survival in host cells as well as in flagellar synthesis (Wang et al., 2022) and characterised as a “division of labor” mechanism (Brameyer et al., 2022). The stop codon and downregulation of *sthE* in ACV could indicate a reduced capability of shedding or biofilm formation, while increasing mechanisms that adapt to stress and host immune responses.

The gene *oadB* (oxaloacetate decarboxylase beta chain), essential for anaerobic respiration, exhibits a stop codon in the ACV strain, suggesting a likely disruption of its function within this pathway. Although *oadB* was initially omitted from our network analysis due to its isolated status, closer examination reveals a connection to *fumB* (fumarase B) through the intermediate gene *purU*. In the ACV strain, *fumB* is notably upregulated, potentially compensating for the loss of *oadB* function and sustaining anaerobic respiration under altered metabolic conditions. This adaptive shift implies that ACV may have restructured its pathways to reduce reliance on *oadB*, instead enhancing *fumB*-mediated reactions to preserve anaerobic function. Such metabolic flexibility aligns with previous studies linking *oadB* mutations to stress adaptations, particularly under acidic conditions (Ghoshal et al., 2023).

Similarly, we identified a stop codon in *ccmF* (cytochrome c-type biogenesis protein), which implies a loss of function in this gene. This observation is consistent with findings in *Salmonella* Pullorum, where pseudogenization of the *ccm* operon, including *ccmF*, has been linked to adaptation for an extraintestinal lifestyle, reducing dependency on pathways that require cytochrome *c* maturation (Batista et al., 2015). In ACV, the truncation of *ccmF* likely signifies a metabolic shift away from cytochrome *c*-dependent processes, allowing adaptation to environments where these pathways are less critical. Despite this pseudogenization, the *ccm* operon remains upregulated in ACV, though the reasons behind this unexpected expression pattern are currently unknown.

A point mutation with a SIFT score close to 0.00 was found in *cysG* that shows the highest number of connections to other genes or proteins in the computed network defining it as a so-called “hub gene”. *cysG* is a uroporphyrinogen-III C-methyltransferase that produces siroheme, which is used by siroheme-dependent reductases and is involved in the reduction of sulfite to sulfide (Murphy and Siegel, 1973; Pennington et al., 2020). *cysG* showed a nonsense mutation in ACV, an upregulation in the transcriptomic data, and stronger downregulation in the proteomic data. Barrett and Clark (1987) reported that a *cysG* mutant, lacking siroheme, did not reduce sulfite to H₂S. However, this mutant was able to produce H₂S from thiosulfate. This suggests that decreased siroheme production could directly impact the activity of the *asr* operon (*asrABC*),

which is involved in siroheme-dependent anaerobic sulfite reduction (Anantharaman et al., 2018). Accordingly, the ACV also showed downregulation of all three *asr* genes (*asrABC*), however, these genes were below the chosen threshold of 1.5 and thus not included in the Cytoscape network.

Interestingly, the only other H₂S-negative *Salmonella* isolate reported to lack the ability to produce H₂S due to a *cys* mutation also belonged to the serovar group *S. Infantis* – specifically, an isolate with a *cysJ* mutation (Lee et al., 2020). This observation supports the conclusion that in *S. Infantis*, mutations in *cys* genes involved in the sulfate reduction pathway, such as *cysG* and *cysJ*, can result in the inability to produce H₂S. Increased expression of *cysP* (thiosulfate transport protein) and upregulation of *ccm* responsible for heme transport (*ccmA*, *ccmB*, *ccmC*, *ccmD*, *ccmE-2*, *ccmF*, *ccmG*, *ccmH-2*) could suggest a compensatory mechanism by the bacteria. This upregulation of the *ccm* operon, essential for heme transport, has also been observed in *Salmonella* Newport in response to the disinfectant peracetic acid (PAA) (Melanie Smith, 2018), reinforcing the hypothesis that the *ccm* operon may play a role in stress adaptation. Moreover, cytochrome *c3* was reported to be the electron carrier for thiosulfate reductase activities in other bacteria (Barrett and Clark, 1987). Recently, it was shown that cytochrome *c* also plays an essential role in the pathogenicity of *S. Typhimurium* and could potentially play a role in the intra- and extracellular lifestyle change of *Salmonella* by the release of cytochrome *c* into the cytosol (Liu et al., 2024). Thus, the upregulation of the *ccm* operon in our case may represent an adaptive response, potentially linked to environmental stress resilience and pathogenicity.

The mutation in *cysG* in ACV can be directly connected to the cobalamin biosynthesis pathway encoded by the *cbi* operon (synthesis of vitamin B12 adenosyl cobalamide precursor), as it is involved in downstream regulation. Cobalamin, or Vitamin B12, is used in *Salmonella* as a cofactor for additional metabolic pathways necessary for pathogen growth in the intestinal tract (Rowley and Kendall, 2019). In the proteomic data, we observed an upregulation of *cbi* genes (*cbiA*, *cbiC*, *cbiD*, *cbiG*, *cbiH*, *cbiF*, *cbiL*), which was further connected to an upregulation of the *pdu* (propanediol utilization) genes. In *Salmonella*, the *pdu* and *eut* (ethanolamine utilization) operons are used to produce catabolic bacterial microcompartments, which helps *Salmonella* to optimize specific metabolic pathways, such as the degradation of 1, 2-propanediol and ethanolamine, as carbon sources for tetrathionate respiration, providing a competitive advantage in the inflamed intestine (Price-Carter et al., 2001; Thiennimitt et al., 2011).

The proteomic data of the ACV showed an upregulation of the *pdu* gene cluster (*pduA*, *pduC*, *pduD*, *pduE*, *pduG*, *pduJ*, *pduK*, *pduL*, *pduO*) together with a downregulation of the *eut* gene cluster (*eutB*, *eutC*, *eutL*, *eutM*, *eutQ*). The *pdu* genes are involved in processing 1,2-propanediol, while the *eut* genes are responsible for ethanolamine degradation. A study by Sturms et al. (2015) showed that *Salmonella* prefers the usage of 1,2-propanediol over ethanolamine and that the presence of 1,2-propanediol even prevents induction of the *eut* operon, which explains the opposing regulation of these two gene clusters in the ACV. Jakobson and Tullman-Ercek (2016) hypothesized that the usage of bacterial microcompartments is part of a host-associated lifestyle, and that *Salmonella* develops subpopulations depending on the need to either invade intestinal host cells or proliferate and spread. Further explanations for the downregulation of the *eut* gene cluster in *Salmonella* includes the exposure to oxygen stress such as H₂O₂ (Liu et al., 2020) or survival within the host and adaptation to low-oxygen environments regulated by the fumarate and nitrate reduction regulator gene (*fnr*) (Behera et al., 2020). It was not only that *fnr* negatively regulates the *eut* operon as an adaptation mechanism to anaerobic environments but also leads to an upregulation of *fis*, which goes in line with the results of ACV. Additionally, *fnr* is known to be involved in nitrate metabolism. In the ACV, nitrogen metabolism was one of the biggest functional groups, giving the most uniform result. All genes with a significant change in the ACV being categorized under nitrogen metabolism showed an upregulation.

The gene *dcm* encoding DNA cytosine methylase showed a missense mutation with a low SIFT score in ACV, which was also confirmed by transcriptome analysis. In *E. coli*, *dcm* has been reported to regulate stationary phase gene expression (Kahramanoglou et al., 2012). Another study by Militello et al. (2014) revealed increased antimicrobial resistance in a *dcm* knockout strain. A review article by Papaleo et al. (2022) connected DNA methylation with bacterial mutation due to exposure to antimicrobial compounds. Other genes of DNA mismatch repair systems, such as *mutM* (formamidopyrimidine DNA glycosylase), *holB* (DNA polymerase III, delta prime subunit), and *xseB* (exonuclease VII, small subunit), were upregulated in the ACV and are known to play a role in adapting to environmental changes and stress response (Pinilla et al., 2022; Qi et al., 2023). These findings suggest that environmental stressors or exposure to antimicrobials may have induced mutations in *dcm*, leading to altered DNA methylation and genomic instability. Consequently, the activation of DNA repair pathways could have facilitated additional mutations, including those responsible for the ACV phenotype.

A missense mutation of *ompF* (outer membrane protein 1a) in the ACV is reinforced by downregulation in both the transcriptome and proteome as well as a low SIFT score. *ompF* encodes a porin in *Salmonella* that mediates the inflow of nutrients and antimicrobial drugs (Wu et al., 2023). This porin is regulated by a two-component system, EnvZ-OmpR, and is influenced by environmental conditions. It is known to be downregulated in *Salmonella* exposed to antimicrobials as well as to acid or oxidative stress (Liu et al., 2020; Trampari et al., 2022; Vidovic et al., 2019; Wu et al., 2023). It has been shown that *ompF* mutants are often associated with increased resistance against antimicrobials such as cefoxitin which is supported by the phenotypic resistance of the ACV against cefoxitin (Montoro-Dasi et al., 2023; Zhou et al., 2023a,b). In the cluster connected to the downregulation of *ompF* is *yfeA* (diguanylate cyclase), a phosphodiesterase, showing a missense variant in the genome and downregulation in both transcriptomic and proteomic data. Activation of *yfeA* leads to reduced c-di-GMP levels, thereby reducing cellulose secretion and cellular aggregation, which influences motility, sessility behaviour, and biofilm formation (Stern et al., 2022). The network computed shows a direct connection from the downregulated *ompF* to an upregulation of *fliB* (filament structural protein) and downregulation of *fliC* (flagellar biosynthesis protein). This indicates a flagellar switch, decreasing flagellin expression, which can be explained by *Salmonella* escaping host immune response after cell invasion (Ma et al., 2022; Wang et al., 2022).

A missense variation in the gene *ygbD*, also known as *norW* and encoding a putative oxidoreductase, was connected to an upregulation in the transcriptomic data. This gene is linked to the upregulation of other oxidoreductase genes, such as *hcr* and *ndh*, and to the downregulation of *zraP*, which is involved in zinc resistance. Upregulation of *ygbD/norW* has been associated with oxidative stress and was reported in *S. Enteritidis* after sodium hypochlorite treatment (Wang et al., 2022) and indicates once more that the development of an ACV phenotype is most likely a consequence of environmental stress.

The persistence of *Salmonella* within the host's intestine relies on diverse strategies that allow it to outcompete microbiota, invade host epithelial cells, and persist within intracellular vacuoles (Li et al., 2023). One important strategy is the production and utilization of H₂S, which *Salmonella* uses for anaerobic respiration within the inflamed gut environment (Winter et al., 2010). *Salmonella* is also well known for its ability to adapt to environmental changes and stress, resulting in alternate phenotypes and highlights the capability of *Salmonella* to increase its persistence and develop subpopulations exhibiting new features (Ackermann, 2015). Such mechanisms, as "division of labour" and "bet-hedging", are used by *Salmonella* to ensure survival within the host by minimising functions which are not of utmost necessity (Arnoldini et al., 2014; Grimbergen et al., 2015; Morawska et al., 2022). These adaptation abilities could explain the heterogenous phenotype and the switch to an ACV lacking H₂S production potentially due to

antimicrobial exposure, disinfectants, or environmental stress within the host. The *S. Infantis* ACV showed changes in only 15 genes and a similar finding was reported in *S. Typhimurium* with heterogenous phenotypes diverging from each other with less than 12 SNPs (Gebremichael et al., 2022). The variants found by Gebremichael et al. (2022) showed, beside diverging phenotypes, also changes in the antimicrobial resistances, underscoring the clinical implications of treating infections as if they are single-cell populations as it can lead to ineffective therapy outcomes. Furthermore, such atypical phenotypes could pass undetected official screening methods and thus be of substantial risk for the public health (Hess et al., 2023).

5. Conclusion

We identified a *S. Infantis* isolate that exhibited an H₂S-negative phenotype (ACV) in the field. Based on the results of multi-omics analyses, we demonstrated that ACV is a variant derived from NCP likely as a result of adaptation mechanisms to environmental changes such as oxidative stress caused by using antimicrobials or disinfectants or due to host-pathogen interactions. This adaptation involved the downregulation of energy-consuming processes, such as H₂S production, which is essential for outcompeting other bacteria in the intestine. Additionally, the ACV acquired resistance against cefoxitin and showed upregulation of pathways necessary for an intracellular lifestyle, such as evading the host immune response.

CRedit authorship contribution statement

Victoria Drauch: Writing – original draft, Visualization, Methodology, Investigation, Data curation, Conceptualization. **Nicola Palmieri:** Writing – review & editing, Visualization, Methodology, Data curation. **Joachim Spersger:** Writing – review & editing, Supervision, Methodology, Conceptualization. **Karin Hummel:** Writing – review & editing, Visualization, Validation, Investigation. **Marlene Brandstetter:** Writing – review & editing, Visualization, Validation, Investigation. **Christian Kornschober:** Writing – review & editing, Validation, Resources, Investigation. **Michael Hess:** Writing – review & editing, Resources, Project administration, Conceptualization. **Claudia Hess:** Writing – review & editing, Supervision, Project administration, Funding acquisition, Conceptualization.

Declaration of competing interest

The authors declare the following financial interests/personal relationships which may be considered as potential competing interests: Victoria Drauch reports financial support was provided by Republic of Austria Federal Ministry of Agriculture Regions and Tourism. If there are other authors, they declare that they have no known competing financial interests or personal relationships that could have appeared to influence the work reported in this paper.

Acknowledgments

This project was funded by the Austrian Federal Ministry Republic of Austria Agriculture, Regions and Tourism together with the Austrian Federal Ministry Republic of Austria Social Affairs, Health, Care and Consumer Protection (grant number 101365). The research was supported using resources of the VetCore Facility (Mass Spectrometry/ Transcriptomics) of the University of Veterinary Medicine Vienna. The Vienna BioCenter Core Facilities (VBCF) Electron Microscopy Facility acknowledges funding from the Austrian Federal Ministry of Education, Science & Research, and the City of Vienna.

Appendix A. Supplementary data

Supplementary data to this article can be found online at <https://doi.org/10.1016/j.fm.2025.104744>.

[org/10.1016/j.fm.2025.104744](https://doi.org/10.1016/j.fm.2025.104744).

References

- Abd El Ghany, Moataz, Shi, Xiaolu, Li, Yinghui, Ansari, Hifzur R., Hill-Cawthorne, Grant A., Ho, Y.S., et al., 2016. Genomic and phenotypic analyses reveal the emergence of an atypical *Salmonella enterica* serovar Senftenberg variant in China. *J. Clin. Microbiol.* 54 (8), 2014–2022. <https://doi.org/10.1128/JCM.00052-16>.
- Ackermann, Martin, 2015. A functional perspective on phenotypic heterogeneity in microorganisms. *Nat. Rev. Microbiol.* 13 (8), 497–508. <https://doi.org/10.1038/nrmicro3491>.
- Alba, Patricia, Leekitcharoenphon, Pimlapas, Carfora, Virginia, Amoroso, Roberta, Cordaro, Gessica, Matteo, Di, Paola, et al., 2020. Molecular epidemiology of *Salmonella infantis* in Europe: insights into the success of the bacterial host and its parasitic pESI-like megaplasmid. *Microb. Genom.* 6 (5). <https://doi.org/10.1099/mgen.0.000365>.
- Albert, M. John, Obaid, Al, Khaled, Alfouzan, Wadha, Sheikh, Rashid, Abdul, Udo, Edet, Izumiya, Hidemasa, et al., 2014. Isolation of *Salmonella enterica* serovar Kentucky strain ST 198 and its H2S-negative variant from a patient: implications for diagnosis. *J. Clin. Microbiol.* 52 (11), 4090–4093. <https://doi.org/10.1128/JCM.01775-14>.
- Altenhoff, Adrian M., Levy, Jeremy, Zarowiecki, Magdalena, Tomiczek, Bartomiej, Warwick, Vesztrocy, Alex, Dalquen, Daniel A., et al., 2019. OMA standalone: orthology inference among public and custom genomes and transcriptomes. *Genome Res.* 29 (7), 1152–1163. <https://doi.org/10.1101/gr.243212.118>.
- Alvarez, Diana M., Barrón-Montenegro, Rocío, Conejeros, José, Rivera, Dácil, Undurraga, Eduardo A., Moreno-Switt, Andrea L., 2023. A review of the global emergence of multidrug-resistant *Salmonella enterica* subsp. *enterica* Serovar *infantis*. *Int. J. Food Microbiol.* 403, 110297. <https://doi.org/10.1016/j.ijfoodmicro.2023.110297>.
- Anantharaman, Karthik, Hausmann, Bela, Jungbluth, Sean P., Kantor, Rose S., Lavy, Adi, Warren, Lesley A., et al., 2018. Expanded diversity of microbial groups that shape the dissimilatory sulfur cycle. *ISME J.* 12 (7), 1715–1728. <https://doi.org/10.1038/s41396-018-0078-0>.
- Arnoldini, Markus, Vizcarra, Ima Avalos, Peña-Miller, Rafael, Stocker, Nicolas, Diard, Médéric, Vogel, Viola, et al., 2014. Bistable expression of virulence genes in *Salmonella* leads to the formation of an antibiotic-tolerant subpopulation. *PLoS Biol.* 12 (8), e1001928. <https://doi.org/10.1371/journal.pbio.1001928>.
- Barrett, E.L., Clark, M.A., 1987. Tetrathionate reduction and production of hydrogen sulfide from thiosulfate. *Microbiol. Rev.* 51 (2), 192–205. <https://doi.org/10.1128/mr.51.2.192-205.1987>.
- Bates, Donna M., Eiff, Christof von, McNamara, Peter J., Peters, Georg, Yeaman, Michael R., Bayer, Arnold S., Proctor, Richard A., 2003. *Staphylococcus aureus* menD and hemB mutants are as infective as the parent strains, but the menadiene biosynthetic mutant persists within the kidney. *J. Infect. Dis.* 187 (10), 1654–1661. <https://doi.org/10.1086/374642>.
- Batista, Diego Felipe Alves, Freitas, Neto, Caetano, Oliveira, Barrow, Paul Andrew, Oliveira, Marcos Túlio de, Almeida, Adriana Maria, Ferraudo, Antonio Sergio, Berchieri, Angelo, 2015. Identification and characterization of regions of difference between the *Salmonella Gallinarum* biovar *Gallinarum* and the *Salmonella Gallinarum* biovar *Pullorum* genomes. *Infect. Genet. Evol.* 30, 74–81. <https://doi.org/10.1016/j.meegid.2014.12.007>.
- Behera, Parthasarathi, Nikhil, K.C., Kumar, Ajay, Gali, Jagan Mohanarao, De, A., Mohanty, A.K., et al., 2020. Comparative proteomic analysis of *Salmonella* Typhimurium wild type and its isogenic fmr null mutant during anaerobiosis reveals new insight into bacterial metabolism and virulence. *Microb. Pathog.* 140, 103936. <https://doi.org/10.1016/j.micpath.2019.103936>.
- Bezek, Katja, Avberšek, Jana, Rojs, Zorman, Olga, Barlič-Maganja, Darja, 2023. Antimicrobial and antibiofilm effect of commonly used disinfectants on *Salmonella infantis* isolates. *Microorganisms* 11 (2). <https://doi.org/10.3390/microorganisms11020301>.
- Brameyer, Sophie, Schumacher, Kilian, Kuppermann, Sonja, Jung, Kirsten, 2022. Division of labor and collective functionality in *Escherichia coli* under acid stress. *Commun. Biol.* 5 (1), 327. <https://doi.org/10.1038/s42003-022-03281-4>.
- Cano, David A., Pucciarelli, M. Graciela, Martínez-Moya, Marina, Casadesús, Josep, García-del Portillo, Francisco, 2003. Selection of small-colony variants of *Salmonella enterica* serovar typhimurium in nonphagocytic eucaryotic cells. *Infect. Immun.* 71 (7), 3690–3698. <https://doi.org/10.1128/IAI.71.7.3690-3698.2003>.
- Cingolani, Pablo, Platts, Adrian, Le Wang, Lily, Coon, Melissa, Nguyen, Tung, Wang, Luan, et al., 2012. A program for annotating and predicting the effects of single nucleotide polymorphisms. SnpEff: SNPs in the genome of *Drosophila melanogaster* strain w1118; iso-2; iso-3. *Fly* 6 (2), 80–92. <https://doi.org/10.4161/fly.19695>.
- Clark, M.A., Barrett, E.L., 1987. The pbs gene and hydrogen sulfide production by *Salmonella typhimurium*. *J. Bacteriol.* 169 (6), 2391–2397. <https://doi.org/10.1128/jb.169.6.2391-2397.1987>.
- CLSI, 2015. Performance Standards for Antimicrobial Disk and Dilution Susceptibility Tests for Bacteria Isolated from Animals, third ed., VET01S
- Colombe, Soledad, Jernberg, Cecilia, Löf, Emma, Angervall, Anna Lindqvist, Mellström-Dahlgen, Henrik, Dotevall, Leif, et al., 2019. Outbreak of Unusual H2S-Negative Monophasic *Salmonella Typhimurium* Strain Likely Associated with Small Tomatoes. Sweden, August to October 2019.
- Drauch, Victoria, Ibesich, Claudia, Vogl, Claus, Hess, Michael, Hess, Claudia, 2020. In vitro testing of bacteriostatic and bactericidal efficacy of commercial disinfectants against *Salmonella infantis* reveals substantial differences between products and bacterial strains. *Int. J. Food Microbiol.* 328, 108660. <https://doi.org/10.1016/j.ijfoodmicro.2020.108660>.
- Drauch, V., Mitra, T., Liebhart, D., Hess, M., Hess, C., 2022. Infection dynamics of *Salmonella infantis* vary considerably between chicken lines. *Avian Pathol.* 51 (6), 561–573. <https://doi.org/10.1080/03079457.2022.2108373>.
- Drescher, Samara Paula Mattiello, Gallo, Stephanie Wagner, Ferreira, Pedro Maria, Abreu, Ferreira, Carlos Alexandre Sanchez, Oliveira, Sílvia Dias de, 2019. *Salmonella enterica* persister cells form unstable small colony variants after in vitro exposure to ciprofloxacin. *Sci. Rep.* 9 (1), 7232. <https://doi.org/10.1038/s41598-019-43631-7>.
- EFSA and ECDC, 2024. The European union one health 2023 zoonoses report. *EFSA J. Europ. Food Safety Author.* 22 (12), e9106. <https://doi.org/10.2903/j.efsa.2024.9106>.
- Eran, Zeynep, Akçelik, Mustafa, Yazıcı, Betül Cansu, Özcengiz, Gülay, Akçelik, Nefise, 2020. Regulation of biofilm formation by marT in *Salmonella Typhimurium*. *Mol. Biol. Rep.* 47 (7), 5041–5050. <https://doi.org/10.1007/s11033-020-05573-6>.
- Gebremichael, Yismashoa, Crandall, John, Mukhopadhyay, Rituparna, Xu, Fengfeng, 2022. *Salmonella* subpopulations identified from human specimens express heterogeneous phenotypes that are relevant to clinical diagnosis. *In: Microbiology Spectrum*, e0167922. <https://doi.org/10.1128/spectrum.01679-22>.
- Ghoshal, Mrinalini, Bechtel, Tyler D., Gibbons, John G., McLandsborough, Lynne, 2023. Adaptive laboratory evolution of *Salmonella enterica* in acid stress. *In: Frontiers in Microbiology*, vol. 14, 1285421. <https://doi.org/10.3389/fmicb.2023.1285421>.
- Greninger, Alexander L., Addetia, Amin, Tao, Yue, Adler, Amanda, Qin, Xuan, 2021. Inactivation of genes in oxidative respiration and iron acquisition pathways in pediatric clinical isolates of Small colony variant Enterobacteriaceae. *Sci. Rep.* 11 (1), 7457. <https://doi.org/10.1038/s41598-021-86764-4>.
- Grimbergen, Ard Jan, Siebring, Jeroen, Solopova, Ana, Kuipers, Oscar P., 2015. Microbial bet-hedging: the power of being different. *In: Current Opinion in Microbiology*, vol. 25, pp. 67–72. <https://doi.org/10.1016/j.cmi.2015.04.008>.
- Hess, Claudia, Drauch, Victoria, Spersger, Joachim, Kornschöber, Christian, Hess, Michael, 2023. Detection of atypical *Salmonella infantis* phenotypes in broiler environmental samples. *Microbiol. Spectr.* 11 (3), e0010623. <https://doi.org/10.1128/spectrum.00106-23>.
- ISO 6579-1, 2017. ISO: ISO 6579-1.
- Jakobson, Christopher M., Tullman-Ereck, Danielle, 2016. Dumpster diving in the gut: bacterial microcompartments as part of a host-associated lifestyle. *PLoS Pathog.* 12 (5), e1005558. <https://doi.org/10.1371/journal.ppat.1005558>.
- Kahramanoglu, Christina, Prieto, Ana I., Khedkar, Supriya, Haase, Bettina, Gupta, Ankur, Benes, Vladimir, et al., 2012. Genomics of DNA cytosine methylation in *Escherichia coli* reveals its role in stationary phase transcription. *In: Nature Communications*, vol. 3, p. 886. <https://doi.org/10.1038/ncomms1878>.
- Kovac, Jasna, Cummings, Kevin J., Rodriguez-Rivera, Lorraine D., Carroll, Laura M., Thachil, Anil, Wiedmann, Martin, 2017. Temporal genomic phylogeny reconstruction indicates a geospatial transmission path of *Salmonella enterica* serovar typhimurium and a clade-specific loss of hydrogen sulfide production. *In: Front. Microbiol.*, vol. 8. <https://doi.org/10.3389/fmicb.2017.00737>. Article 737.
- Kwan, H.S., Barrett, E.L., 1983. Roles for menaquinone and the two trimethylamine oxide (TMAO) reductases in TMAO respiration in *Salmonella typhimurium*: mu d (Apr lac) insertion mutations in men and tor. *J. Bacteriol.* 155 (3), 1147–1155. <https://doi.org/10.1128/jb.155.3.1147-1155.1983>.
- Kwan, H.S., Barrett, E.L., 1984. Map locations and functions of *Salmonella typhimurium* men genes. *J. Bacteriol.* 159 (3), 1090–1092. <https://doi.org/10.1128/jb.159.3.1090-1092.1984>.
- Lee, Kwang Seob, Kim, Daewon, Lee, Hyukmin, Lee, Kyungwon, Yong, Dongeun, 2020. Isolation of non-hydrogen sulfide-producing *Salmonella enterica* serovar infantis from a clinical sample: the first case in Korea. *Ann. Lab. Med.* 40 (4), 334–336. <https://doi.org/10.3343/alm.2020.40.4.334>.
- Li, Wanli, Li, Yinghui, Wu, Yarong, Cui, Yujun, Liu, Yao, Shi, Xiaolu, et al., 2016. Phenotypic and genetic changes in the life cycle of small colony variants of *Salmonella enterica* serotype Typhimurium induced by streptomycin. *Ann. Clin. Microbiol. Antimicrob.* 15 (1), 37. <https://doi.org/10.1186/s12941-016-0151-3>.
- Li, Wanwu, Ren, Qili, Ni, Ting, Zhao, Yifei, Sang, Zichun, Luo, Renli, et al., 2023. Strategies adopted by *Salmonella* to survive in host: a review. *Arch. Microbiol.* 205 (12), 362. <https://doi.org/10.1007/s00203-023-03702-w>.
- Liu, Xiaoying, Omar, Misara, Abrahante, Juan E., Nagaraja, Kakambi V., Vidovic, Sinisa, 2020. Insights into the oxidative stress response of *Salmonella enterica* serovar Enteritidis revealed by the next generation sequencing approach. *Antioxidants* 9 (9). <https://doi.org/10.3390/antiox9090849>.
- Liu, Xingmei, Liu, Yutao, Zhao, Xinyu, Li, Xueping, Yao, Ting, Liu, Ruiying, et al., 2024. *Salmonella enterica* serovar Typhimurium remodels mitochondrial dynamics of macrophages via the T3SS effector SipA to promote intracellular proliferation. *Gut Microbes* 16 (1), 2316932. <https://doi.org/10.1080/19490976.2024.2316932>.
- Ma, Yue, Yue, Yingying, Jia, Haihong, Song, Nannan, Zhai, Li, Wang, Weiwei, et al., 2022. Switching off bacterial flagellar biogenesis by YdiU-mediated UMPylation of FlhDC. *mBio* 13 (3), e0024922. <https://doi.org/10.1128/mbio.00249-22>.
- Mayr, Anna-Lena, Hummel, Karin, Leitsch, David, Razzazi-Fazeli, Ebrahim, 2024. A comparison of bottom-up proteomic sample preparation methods for the human parasite *Trichomonas vaginalis*. *ACS Omega* 9 (8), 9782–9791. <https://doi.org/10.1021/acsomega.3c10040>.
- McMillan, Elizabeth A., Weinroth, Margaret D., Frye, Jonathan G., 2022. Increased prevalence of *Salmonella infantis* isolated from raw chicken and Turkey products in the United States is due to a single clonal lineage carrying the pESI plasmid. *Microorganisms* 10 (7). <https://doi.org/10.3390/microorganisms10071478>.

- Meganathan, R., Kwon, Ohsuk, 2009. Biosynthesis of menaquinone (vitamin K2) and ubiquinone (Coenzyme Q). *EcoSal Plus* 3 (2). <https://doi.org/10.1128/ecosalplus.3.6.3.3>.
- Melanie Smith, Dara, 2018. *Transcriptomic Analysis of Salmonella enterica Newport Adaptive Response to Oxidative Antimicrobials*. University of Tennessee.
- Millitello, Kevin T., Mandarano, Alexandra H., Varchtchouk, Olga, Simon, Robert D., 2014. Cytosine DNA methylation influences drug resistance in *Escherichia coli* through increased *sugE* expression. *FEMS Microbiol. Lett.* 350 (1), 100–106. <https://doi.org/10.1111/1574-6968.12299>.
- Montoro-Dasi, Laura, Lorenzo-Rebenaque, Laura, Marco-Fuertes, Ana, Vega, Santiago, Marin, Clara, 2023. Holistic strategies to control *Salmonella infantis*: an emerging challenge in the European broiler sector. *Microorganisms* 11 (7). <https://doi.org/10.3390/microorganisms11071765>.
- Morawska, Luiza P., Hernandez-Valdes, Jhonatan A., Kuipers, Oscar P., 2022. Diversity of bet-hedging strategies in microbial communities—Recent cases and insights. *WIREs Mech. Dis.* 14 (2), e1544. <https://doi.org/10.1002/wsbm.1544>.
- Mourão, Joana, Rebelo, Andreia, Ribeiro, Sofia, Peixe, Luísa, Novais, Carla, Antunes, Patrícia, 2020. Atypical non-H2S-producing monophasic *Salmonella typhimurium* ST3478 strains from chicken meat at processing stage are adapted to diverse stresses. *Pathogens* 9 (9). <https://doi.org/10.3390/pathogens9090701>.
- Murphy, Matthew J., Siegel, Lewis M., 1973. Siroheme and Sirohydrochlorin. *J. Biol. Chem.* 248 (19), 6911–6919. [https://doi.org/10.1016/S0021-9258\(19\)43436-4](https://doi.org/10.1016/S0021-9258(19)43436-4).
- Müstak, İnci Başak, Müstak, Hamit Kaan, Sarıçam, Seyyide, 2020. Molecular characterisation of hydrogen sulfide negative *Salmonella enterica* serovar Havana. *Antonie Leeuwenhoek* 113 (9), 1241–1246. <https://doi.org/10.1007/s10482-020-01432-3>.
- Nair, Abhilash Vijay, Singh, Anmol, Rajmani, R.S., Chakravorty, Dipshikha, 2024. *Salmonella Typhimurium* employs spermidine to exert protection against ROS-mediated cytotoxicity and rewires host polyamine metabolism to ameliorate its survival in macrophages. In: *Redox Biology*, vol. 72, 103151. <https://doi.org/10.1016/j.redox.2024.103151>.
- Ng, Pauline C., Henikoff, Steven, 2003. SIFT: predicting amino acid changes that affect protein function. *Nucleic Acids Res.* 31 (13), 3812–3814. <https://doi.org/10.1093/nar/gkg509>.
- Papaleo, Stella, Alvaro, Alessandro, Nodari, Riccardo, Panelli, Simona, Bitar, Ibrahim, Comandatore, Francesco, 2022. The red thread between methylation and mutation in bacterial antibiotic resistance: how third-generation sequencing can help to unravel this relationship. In: *Frontiers in Microbiology*, vol. 13, 957901. <https://doi.org/10.3389/fmicb.2022.957901>.
- Pennington, Joseph M., Kemp, Michael, McGarry, Lauren, Chen, Yu, Stroupe, M. Elizabeth, 2020. Siroheme synthase orients substrates for dehydrogenase and chelatase activities in a common active site. *Nat. Commun.* 11 (1), 864. <https://doi.org/10.1038/s41467-020-14722-1>.
- Pinilla, Cristian Mauricio Barreto, Stincone, Paolo, Brandelli, Adriano, 2022. Proteomic dataset of *Listeria monocytogenes* exposed to sublethal concentrations of free and nanoencapsulated nisin. In: *Data in Brief*, vol. 43, 108343. <https://doi.org/10.1016/j.dib.2022.108343>.
- Powers, TuShun R., Haerberle, Amanda L., Predeus, Alexander V., Hammarlöf, Disa L., Cundiff, Jennifer A., Saldana-Ahuactzi, Zeus, et al., 2021. Intracellular niche-specific profiling reveals transcriptional adaptations required for the cytosolic lifestyle of *Salmonella enterica*. *PLoS Pathog.* 17 (8), e1009280. <https://doi.org/10.1371/journal.ppat.1009280>.
- Pränting, Maria, Andersson, Dan I., 2010. Mechanisms and physiological effects of protamine resistance in *Salmonella enterica* serovar Typhimurium LT2. *J. Antimicrob. Chemother.* 65 (5), 876–887. <https://doi.org/10.1093/jac/dkq059>.
- Price-Carter, M., Tingey, J., Bobik, T.A., Roth, J.R., 2001. The alternative electron acceptor tetrathionate supports B12-dependent anaerobic growth of *Salmonella enterica* serovar typhimurium on ethanolamine or 1,2-propanediol. *J. Bacteriol.* 183 (8), 2463–2475. <https://doi.org/10.1128/JB.183.8.2463-2475.2001>.
- Proctor, Richard A., Eiff, Christof von, Kahl, Barbara C., Becker, Karsten, McNamara, Peter, Herrmann, Mathias, Peters, Georg, 2006. Small colony variants: a pathogenic form of bacteria that facilitates persistent and recurrent infections. *Nat. Rev. Microbiol.* 4 (4), 295–305. <https://doi.org/10.1038/nrmicro1384>.
- Qi, Wenxi, Jonker, Martijs J., Leeuw, Wim de, Brul, Stanley, Kuile, Benno H. ter, 2023. Reactive oxygen species accelerate de novo acquisition of antibiotic resistance in *E. coli*. *iScience* 26 (12), 108373. <https://doi.org/10.1016/j.isci.2023.108373>.
- Rowley, Carol A., Kendall, Melissa M., 2019. To B12 or not to B12: five questions on the role of cobalamin in host-microbial interactions. *PLoS Pathog.* 15 (1), e1007479. <https://doi.org/10.1371/journal.ppat.1007479>.
- Sakano, Chieko, Kuroda, Makoto, Sekizuka, Tsuyoshi, Ishioka, Taisei, Morita, Yukio, Ryo, Akihide, et al., 2013. Genetic analysis of non-hydrogen sulfide-producing *Salmonella enterica* serovar typhimurium and *S. enterica* serovar infantis isolates in Japan. *J. Clin. Microbiol.* 51 (1), 328–330. <https://doi.org/10.1128/JCM.02225-12>.
- Stern, Einav, Shterzer, Naama, Mills, Erez, 2022. Characterizing 5-oxoproline sensing pathways of *Salmonella enterica* serovar typhimurium. *Sci. Rep.* 12 (1), 15975. <https://doi.org/10.1038/s41598-022-20407-0>.
- Sturms, Ryan, Streauslin, Nicholas A., Cheng, Shouqiang, Bobik, Thomas A., 2015. In *Salmonella enterica*, ethanolamine utilization is repressed by 1,2-propanediol to prevent detrimental mixing of components of two different bacterial microcompartments. *J. Bacteriol.* 197 (14), 2412–2421. <https://doi.org/10.1128/JB.00215-15>.
- Thiennimitr, Parameth, Winter, Sebastian E., Winter, Maria G., Xavier, Mariana N., Tolstikov, Vladimir, Huseby, Douglas L., et al., 2011. Intestinal inflammation allows *Salmonella* to use ethanolamine to compete with the microbiota. *Proc. Natl. Acad. Sci. U. S. A.* 108 (42), 17480–17485. <https://doi.org/10.1073/pnas.1107857108>.
- Tonkin-Hill, Gerry, MacAlasdair, Neil, Ruis, Christopher, Weimann, Aaron, Horesh, Gal, Lees, John A., et al., 2020. Producing polished prokaryotic pangenomes with the Panaroo pipeline. *Genome Biol.* 21 (1), 180. <https://doi.org/10.1186/s13059-020-02090-4>.
- Trampari, Eleftheria, Zhang, Chuangzhen, Gotts, Kathryn, Savva, George M., Bavro, Vassily N., Webber, Mark, 2022. Cefotaxime exposure selects mutations within the CA-domain of *envZ* which promote antibiotic resistance but repress biofilm formation in *Salmonella*. *Microbiol. Spectr.* 10 (3), e0214521. <https://doi.org/10.1128/spectrum.02145-21>.
- Treangen, Todd J., Ondov, Brian D., Koren, Sergey, Phillippy, Adam M., 2014. The Harvest suite for rapid core-genome alignment and visualization of thousands of intraspecific microbial genomes. *Genome Biol.* 15 (11), 524. <https://doi.org/10.1186/s13059-014-0524-x>.
- Vidovic, Sinisa, An, Ran, Rendahl, Aaron, 2019. Molecular and physiological characterization of fluoroquinolone-highly resistant *Salmonella* Enteritidis strains. *Front. Microbiol.* 10, 729. <https://doi.org/10.3389/fmicb.2019.00729>.
- Wang, Sheng, Xiao, Xingning, Qiu, Mengjia, Wang, Wensi, Xiao, Yingping, Yang, Hua, et al., 2022. Transcriptomic responses of *Salmonella enterica* serovar Enteritidis in sodium hypochlorite. In: *Frontiers in Cellular and Infection Microbiology*, vol. 12, 853064. <https://doi.org/10.3389/fcimb.2022.853064>.
- Wang, Weiwei, Yue, Yingying, Zhang, Min, Song, Nannan, Jia, Haihong, Dai, Yuanji, et al., 2022. Host acid signal controls *Salmonella* flagella biogenesis through CadC-YdIV axis. *Gut Microbes* 14 (1), 2146979. <https://doi.org/10.1080/19490976.2022.2146979>.
- Weening, Eric H., Barker, Jared D., Laarakker, Marijke C., Humphries, Andrea D., Tsolis, Renée M., Bäuml, Andreas J., 2005. The *Salmonella enterica* serotype Typhimurium *lpf*, *bcf*, *stb*, *stc*, *std*, and *sth* fimbrial operons are required for intestinal persistence in mice. *Infect. Immun.* 73 (6), 3358–3366. <https://doi.org/10.1128/IAI.73.6.3358-3366.2005>.
- Wick, Ryan R., Judd, Louise M., Gorrie, Claire L., Holt, Kathryn E., 2017. Unicycler: resolving bacterial genome assemblies from short and long sequencing reads. *PLoS Comput. Biol.* 13 (6), e1005595. <https://doi.org/10.1371/journal.pcbi.1005595>.
- Winter, Sebastian E., Thiennimitr, Parameth, Winter, Maria G., Butler, Brian P., Huseby, Douglas L., Crawford, Robert W., et al., 2010. Gut inflammation provides a respiratory electron acceptor for *Salmonella*. *Nature* 467 (7314), 426–429. <https://doi.org/10.1038/nature09415>.
- Wu, Fuli, Xu, Xuebin, Xie, Jing, Yi, Shengjie, Wang, Jian, Yang, Xiaoxia, et al., 2016. Molecular characterization of *Salmonella enterica* serovar Aberdeen negative for H2S production in China. *PLoS One* 11 (8), e0161352. <https://doi.org/10.1371/journal.pone.0161352>.
- Wu, Shang, Ji, Jian, Carole, Nanfack V.D., Yang, Jia, Yang, Yang, Sun, Jiadi, et al., 2023. Combined metabolomics and transcriptomics analysis reveals the mechanism of antibiotic resistance of *Salmonella enterica* serovar Typhimurium after acidic stress. In: *Food Microbiology*, vol. 115, 104328. <https://doi.org/10.1016/j.fm.2023.104328>.
- Xie, Jing, Wu, Fuli, Xu, Xuebin, Yang, Xiaoxia, Zhao, Rongtao, Ma, Qiuxia, et al., 2018. Antibiotic resistance and molecular characterization of the hydrogen sulfide-negative phenotype among diverse *Salmonella* serovars in China. *BMC Infect. Dis.* 18 (1), 292. <https://doi.org/10.1186/s12879-018-3209-3>.
- Yi, Shengjie, Xie, Jing, Liu, Nan, Li, Peng, Xu, Xuebin, Li, Hao, et al., 2014. Emergence and prevalence of non-H2S-producing *Salmonella enterica* serovar Senftenberg isolates belonging to novel sequence type 1751 in China. *J. Clin. Microbiol.* 52 (7), 2557–2565. <https://doi.org/10.1128/JCM.00377-14>.
- Zhou, Gang, Wang, Qian, Wang, Yingsi, Wen, Xia, Peng, Hong, Peng, Ruqun, et al., 2023a. Outer membrane porins contribute to antimicrobial resistance in gram-negative bacteria. *Microorganisms* 11 (7). <https://doi.org/10.3390/microorganisms11071690>.
- Zhou, Kaixiang, Sun, Lei, Zhang, Xuehua, Xu, Xiangyue, Mi, Kun, Ma, Wenjin, et al., 2023b. *Salmonella* antimicrobials inherited and the non-inherited resistance: mechanisms and alternative therapeutic strategies. In: *Frontiers in Microbiology*, vol. 14, 1176317. <https://doi.org/10.3389/fmicb.2023.1176317>.